

---

# OAo/MITSuME Photometry of Dwarf Novae. II. HV Virginis and OT J012059.6+325545

Akira IMADA,<sup>1,2\*</sup> Keisuke ISOGAI,<sup>3</sup> Takahiro ARAKI,<sup>4</sup> Shunsuke TANADA,<sup>4</sup>  
Kenshi YANAGISAWA,<sup>5</sup> Nobuyuki KAWAI<sup>6</sup>

<sup>1</sup>Hamburger Sternwarte, Universität Hamburg, Gojenbergsweg 112, D-21029 Hamburg, Germany

<sup>2</sup>Kwasan and Hida Observatories, Kyoto University, Yamashina, Kyoto 607-8471, Japan

<sup>3</sup>Department of Astronomy, Kyoto University, Kyoto 606-8502, Japan

<sup>4</sup>Faculty of Science, Kagoshima University, 1-21-30 Korimoto, Kagoshima, Kagoshima 890-0065, Japan

<sup>5</sup>Okayama Astrophysical Observatory, National Astronomical Observatory of Japan, Asakuchi, Okayama 719-0232, Japan

<sup>6</sup>Department of Physics, Tokyo Institute of Technology, Ookayama 2-12-1, Meguro-ku, Tokyo 152-8551, Japan

\*E-mail: \*a\_imada@kusastro.kyoto-u.ac.jp

Received 2017 June 1; Accepted 2017 November 15

## Abstract

We report on multicolor photometry of WZ Sge-type dwarf novae, HV Vir and OT J012059.6+325545 during superoutbursts. These systems show early superhumps with the mean periods of 0.057093(45) d for HV Vir and 0.057147(15) d for OT J012059.6+325545, respectively. The observed early superhumps showed a common feature that the brightness minima correspond to the bluest peaks in color variations, which may be a ubiquitous phenomenon among early superhumps of WZ Sge-type dwarf novae. We confirmed that amplitudes of early superhumps depend on wavelength: amplitudes with longer bandpass filters show larger values. This indicates that the light source of early superhumps is generated at the outer region of the vertically-extended accretion disk. On the other hand, amplitudes of ordinary superhumps are likely to be independent of wavelength. This implies that the superhump light source is geometrically thin. We also examined color variations of ordinary superhumps and found that the bluest peaks in  $g' - I_c$  tend to coincide with the brightness minima, particularly in stage B superhumps. This may reflect that the pressure effect plays a dominant role during stage B superhumps.

**Key words:** accretion, accretion disks — stars: dwarf novae — stars: individual (HV Virginis, OT J012059.6+325545) — stars: novae, cataclysmic variables — stars: oscillations

---

## 1 Introduction

Cataclysmic variables (CVs) are close binary systems that consist of a primary white dwarf and a secondary star. The secondary star fills its Roche lobe, transferring matter into the primary Roche lobe via the inner Lagrangian point (L1). If the magnetic field of the white dwarf is

weak, an accretion disk is formed around the white dwarf (for a review, see, e.g., Warner 1995; Hellier 2001).

Dwarf novae are a subclass of CVs, exhibiting outbursts with recurrent time scales of days to years and amplitudes of 2–8 mag (for a review, see, e.g., Osaki 1996; Lasota 2001; Kato et al. 2004b). The accretion disk

plays a major role on the overall behavior of dwarf novae, which is well explained by the thermal instability model of the accretion disk (Meyer, Meyer-Hofmeister 1981; Smak 1984).

Dwarf novae are further divided into several subclasses according to their light curves (Kato et al. 2004b; Kato et al. 2009). One of the subclasses is SU UMa-type dwarf novae. These show two types of outbursts. One is normal outburst, whose duration is a few days, and the other is superoutburst, whose duration is typically 2 weeks. During the superoutburst, modulations with a rapid rise and slow decline, called (positive) superhumps, are visible. The period of the superhump ( $P_{\text{sh}}$ ) is slightly longer than the orbital period of the system ( $P_{\text{orb}}$ ).<sup>1</sup> Long-term light curves of SU UMa-type dwarf novae are well explained by the combination of the thermal and tidal instability model (Osaki 1989; Osaki, Kato 2013a), and the basic properties of superhumps are understood by tidal dissipation of the eccentricity-deformed precessing accretion disk (Whitehurst 1988; Hirose, Osaki 1990).

It has been widely recognized that some SU UMa-type dwarf novae show unusual behavior in their short and long-term light curves. WZ Sge-type dwarf novae, one of the subclasses of SU UMa-type dwarf novae, show unique properties during superoutburst and quiescence (Kato 2015). Their main characteristic features are that (1) their quiescence is unusually long, sometimes exceeding a decade (Nogami et al. 1997; Kato et al. 2001) (2) the amplitudes of the superoutburst exceed 6 mag (Howell et al. 1995; Ishioka et al. 2001), (3) an early stage of the superoutburst contains double-peaked modulations called early superhumps (Osaki, Meyer 2002; Kato 2002)<sup>2</sup>, (4) they show rebrightening(s) after the termination of the main superoutburst (Patterson et al. 2002; Kato et al. 2004a), and (5) they are absent of normal outbursts (For a comprehensive review, see Kato (2015)). Recent optical transient surveys, such as ASAS (Shappee et al. 2014), MASTER (Lipunov et al. 2010), and CRTS (Drake et al. 2009) have revealed the presence of extensive numbers of candidates for WZ Sge-type dwarf novae. However, most of photometry was performed without filters. This means that we have less information on color and temperature variations in the accretion disk of WZ Sge-type dwarf novae.

Based on extensive photometry during superoutbursts, T.Kato and his colleagues have established the "textbook" behavior of superhump period changes (Kato et al. 2009). According to Kato et al. (2009), the evolution

of the superhump period is composed of three stages: an early stage with a longer and constant superhump period (stage A), a middle stage with positive period derivatives  $P_{\text{dot}} = \dot{P}/P$  (stage B), and a late stage with a shorter and constant period (stage C). Although the majority of SU UMa-type dwarf novae follow the trend described here, some systems show an unusual period evolution of superhumps (Kato et al. 2013a). In order to understand the diversity of superhump period changes, multicolor photometry may be an attractive approach. Indeed, simultaneous optical/near-infrared observations have revealed the presence of the warm accretion disk after the termination of a superoutburst (Uemura et al. 2008), and difference in maximum timings between magnitudes and colors of superhumps (Schoembs, Vogt 1980; Hassall 1985; Isogai et al. 2015).

Here we report on optical-near infrared photometry of HV Vir and optical photometry of OT J012059.6+325545 during superoutbursts by using instruments of Okayama Astrophysical Observatory<sup>3</sup>. In the following subsection, we outline the background of these stars.

## 1.1 HV Virginis

HV Vir is one of well-known WZ Sge-type dwarf novae with magnitudes ranging from 11.5 to 19 (Ritter, Kolb 2003). The system underwent outbursts in 1929, 1939, 1970, 1981, 1992, 2008, and 2016 (Kato 2017). Superhumps and early superhumps were detected during the 1992 superoutburst, from which HV Vir has been recognized as a member of WZ Sge-type dwarf novae (Barwig et al. 1992; Leibowitz et al. 1994; Howell et al. 1995). Kato et al. (2001) derived the mean early superhump period to be  $P_{\text{Esh}} = 0.057085(23)$  d. A photometric campaign of the 2002 superoutburst was carried out by Ishioka et al. (2003), who obtained  $P_{\text{sh}} = 0.058203(1)$  d for superhumps and  $P_{\text{Esh}} = 0.0569(1)$  d for early superhumps, respectively. Ishioka et al. (2003) also derived the rate of the period change during stage B to be  $P_{\text{dot}} = 7.8(7) \times 10^{-5}$ . Kato et al. (2009) obtained  $P_{\text{dot}} = 7.1(1.9) \times 10^{-5}$  for the 2008 superoutburst. Patterson et al. (2003) performed quiescent photometry and derived the orbital period to be  $P_{\text{orb}} = 0.057069(6)$  d. Patterson et al. (2003) also noted the presence of a signal at 11.20 or 12.21 c/d ( $P=0.0893$  or  $0.0819$  d), the origin of which is unknown. Similar periodicities were also reported by Woudt et al. (2012), who observed HV Vir in quiescence in 2010 April. An estimation of the temperature of the white dwarf yielded a cool  $T_{\text{eff}}$  of  $13300 \pm 800$  K (Szkody et al. 2002). A distance to the object is estimated as  $480 \pm 70$  pc (Szkody et al. 2002),  $460(+530, -180)$

<sup>1</sup> Some dwarf novae show negative superhumps, whose period is slightly shorter than  $P_{\text{orb}}$ . Throughout this paper, the term "superhump" means positive superhump.

<sup>2</sup> Throughout this paper, a period of early superhumps is designated as  $P_{\text{Esh}}$ .

<sup>3</sup> <http://www.oao.nao.ac.jp>

pc (Thorstensen 2003), and 300 pc (Patterson 2011), respectively.

Here we report on analyses and results of simultaneous optical-near infrared photometry during the 2008 superoutburst of HV Vir. On 2008 February 14.601 (JD 2454511.101), Rod Stubbings detected an eruption of HV Vir with a visual magnitude of 11.5 ([vsnet-alert 9912])<sup>4</sup>. P. Schmeer reported that HV Vir was fainter than 13.7 on 2008 February 14.139 (JD 2454510.639) ([vsnet-alert 9915]). In combination with these reports, we succeeded in observing from the very onset of the outburst.

## 1.2 OT J012059.6+325545

OT J012059.6+325545 (hereafter, J0120) was discovered by K. Itagaki as a transient object on 2010 November 30.50663 (JD 2455531.00663) with a magnitude of 12.3 ([vsnet-alert 12431]). According to the SDSS DR9 database, quiescent magnitudes are  $u = 20.359$ ,  $g = 20.088$ ,  $r = 20.237$ ,  $i = 20.518$ , and  $z = 21.216$  (Ahn et al. 2012). The object has no 2MASS counterpart within 5 arcsec. A distance to the object is estimated as 355 pc (Kato et al. 2012b). After the discovery of the outburst, VSNET conducted a photometric campaign and detected early superhumps with a mean period of  $P_{\text{Esh}} = 0.057155(5)$  d, from which J0120 was qualified as a WZ Sge-type dwarf nova (Kato et al. 2012a). Nakagawa et al. (2013) reported on simultaneous  $g'$ ,  $R_c$ , and  $i'$  photometry during the 2010–2011 superoutburst. Using a model developed by Uemura et al. (2012), they calculated disk structures during the early superhump stage.

In this paper, we focus mainly on details of color and amplitude variations of early and ordinary superhumps which Nakagawa et al. (2013) did not deal with. We succeeded in detecting stage A superhumps in our data. By using a new method of estimating the mass ratio (Kato, Osaki 2013), we derived the mass ratio of the system for the first time.

## 2 Observations

Time-resolved photometry were performed from 2008 February 14 to March 31 (JD 2454511–2454557, for HV Vir) and from 2010 December 3 to 2011 January 4 (JD 2455533–2455565 for J0120), respectively. We used OAO/MITSuME 50cm-telescope and OAO/ISLE 188-cm telescope. We obtained  $g'$ ,  $R_c$ ,  $I_c$ ,  $H$ , and  $K_s$  bands for HV Vir, while we obtained  $g'$ ,  $R_c$ , and  $I_c$  bands for J0120. OAO/MITSuME 50cm-telescope is a robotic telescope

**Table 1.** Log of optical observations of HV Vir using MITSuME.

Date	JD(start)*	JD(end)*	N <sup>†</sup>
2008 February 15	4512.1196	4512.3684	360
2008 February 16	4513.1156	4513.3681	220
2008 February 17	4514.1111	4514.3638	430
2008 February 18	4515.1103	4515.3658	387
2008 February 19	4516.0684	4516.3685	542
2008 February 20	4517.1018	4517.3707	326
2008 February 21	4518.1024	4518.3470	218
2008 February 22	4519.2506	4519.3710	33
2008 February 23	4520.2479	4520.3149	44
2008 February 26	4523.0950	4523.3655	232
2008 February 27	4524.0904	4524.3600	274
2008 February 28	4525.0821	4525.3472	264
2008 February 29	4526.0988	4526.2114	91
2008 March 1	4527.0560	4527.3569	216
2008 March 2	4528.0954	4528.2019	105
2008 March 3	4529.2393	4529.3154	3
2008 March 4	4530.0827	4530.3550	132
2008 March 5	4531.0996	4531.3552	254
2008 March 6	4532.2276	4532.3553	87
2008 March 7	4533.0977	4533.3540	200
2008 March 8	4534.0887	4534.3519	131
2008 March 11	4537.1575	4537.3261	130
2008 March 12	4538.1493	4538.3242	102
2008 March 14	4540.2031	4540.2988	71
2008 March 15	4541.2082	4541.2899	55
2008 March 16	4542.2523	4542.2772	10
2008 March 17	4543.2471	4543.2873	3
2008 March 31	4557.1926	4557.2003	3

\*JD–2450000 † Number of exposure.

**Table 2.** Log of near-infrared observations of HV Vir using ISLE.

Date	JD(start)*	JD(end)*	N <sup>†</sup>	band <sup>§</sup>
2008 February 14	4511.2348	4511.3461	230	$H$
2008 February 15	4512.1723	4512.2501	123	$H$
2008 February 15	4512.2509	4512.3666	185	$K_s$
2008 February 16	4513.1748	4513.3858	167	$K_s$
2008 February 17	4514.1632	4514.3231	178	$K_s$
2008 February 18	4515.1856	4515.3538	179	$K_s$
2008 February 19	4516.1788	4516.3593	337	$K_s$

\*JD–2450000 † Number of exposure.

§  $H$ :  $H$  band.  $K_s$ :  $K_s$  band.

<sup>4</sup> <http://ooruri.kusastro.kyoto-u.ac.jp/pipermail/vsnet-alert/>. For a review of VSNET, see Kato et al. (2004b)

**Table 3.** Log of observations for J0120.

Date	JD(start)*	JD(end)*	N <sup>†</sup>
2010 December 3	5533.8857	5534.0883	445
2010 December 4	5534.9216	5535.1766	319
2010 December 5	5535.8853	5536.0879	446
2010 December 9	5539.9196	5540.0256	234
2010 December 10	5540.9302	5541.0535	223
2010 December 11	5541.8968	5542.0229	243
2010 December 12	5542.9288	5543.1383	24
2010 December 14	5544.9190	5545.0654	183
2010 December 15	5545.8884	5546.0053	18
2010 December 17	5547.9057	5547.9982	9
2010 December 18	5548.9637	5549.1209	174
2010 December 19	5549.8947	5549.9992	206
2010 December 20	5550.9093	5551.1697	443
2010 December 22	5552.8977	5553.1289	243
2010 December 23	5553.8743	5554.1251	341
2010 December 24	5554.9928	5555.1228	2
2010 December 25	5555.8750	5556.1277	294
2010 December 26	5556.9594	5557.1822	5
2010 December 27	5557.8760	5558.0998	120
2010 December 28	5558.9161	5558.9577	56
2010 December 29	5559.8769	5560.1004	400
2010 December 30	5560.8774	5561.0367	229
2010 December 31	5561.8778	5562.0846	7
2011 January 1	5562.8784	5562.9930	204
2011 January 2	5563.8792	5564.1363	142
2011 January 4	5565.8802	5565.8846	11

\*JD–2450000

†Number of exposure.

that can obtain  $g'$ ,  $R_c$ , and  $I_c$  simultaneously by using two dichroic mirrors and three CCD cameras, which enables us to study color variations of variable stars (For a detail description, see Kotani et al. 2005). ISLE is an instrument that obtains  $J$ ,  $H$ , and  $K_s$  images and medium-resolution spectra, attached with the Cassegrain focus of the OAO 188-cm telescope (Yanagisawa et al. 2006). Table 1, 2, and 3 show the journals of observations. All data were obtained with 30–sec exposures.

After de-biasing, dark-subtracting and flat-fielding the images with the standard procedure, the data were analyzed with aperture photometry using IRAF/daophot.<sup>5</sup> In order to study color variations of  $g' - K_s$ , we interpolated the ISLE magnitudes to the times of MITSuME observations, because there were slight differences of

mid-exposure time between the data of MITSuME and ISLE. We derived magnitudes and colors with differential photometry using SDSS J132054.81+015207.4 ( $g' = 14.286(3)$ ,  $r' = 13.938(4)$ ,  $i' = 13.838(4)$ ) for HV Vir and SDSS J012048.61+325718.1 ( $g' = 12.779(1)$ ,  $r' = 12.522(1)$ ,  $i' = 12.624(2)$ ) for J0120, respectively. The constancy of these comparison stars is checked by nearby stars in the same field. Because the exact magnitudes of  $R_c$  and  $I_c$  of the comparison star are unknown, we converted the SDSS magnitudes to  $R_c$  and  $I_c$  given by Smith et al. (2002) as follows:

$$V = g' - 0.55(g' - r') - 0.03 \quad (1)$$

$$V - R = 0.59(g' - r') + 0.11 \quad (2)$$

$$R - I = 1.00(r' - i') + 0.21 \quad (3)$$

Using the above equations and 2MASS archives, we adopt  $g' = 14.286(3)$ ,  $R_c = 13.749(5)$ ,  $I_c = 13.439(5)$ ,  $H = 12.716(25)$ , and  $K_s = 12.686(27)$  as the magnitudes of the comparison star of HV Vir. As for the magnitudes of the comparison star of J0120, we adopt  $g' = 12.779(1)$ ,  $R_c = 12.346(1)$  and  $I_c = 12.238(2)$ . Barycentric correction was made before the following analyses.

## 3 Results of HV Vir

### 3.1 overall light curves

Figure 1 shows the light curves of HV Vir during our run. As can be seen in figure 1, the plateau stage lasted for 20 d, which was a usual value for WZ Sge-type dwarf novae (Kato 2015). Although WZ Sge-type dwarf novae frequently show rebrightenings (Patterson et al. 1998), the present observations provided no evidence for rebrightenings. The absence of rebrightenings is also confirmed in the 1992 and 2016 superoutbursts of the same object (Leibowitz et al. 1994; Kato 2017). These superoutbursts can be categorized into the type-D classification (no rebrightenings) introduced by Imada et al. (2006) and Kato (2015).

Representative light curves in early phase of the superoutburst are given in figure 2, in which the characteristic features of early and ordinary superhumps are visible. As illustrated in figure 2, superhumps appeared on 2008 February 20 (JD 2454517). This means that the superhumps appeared on the 6th day after the beginning of the superoutburst. In conjunction with the reported visual observations, the early superhumps of HV Vir lasted for 6 d. Superhumps sustained after the end of the plateau stage. This phenomenon is common among WZ Sge-type dwarf novae (Kato et al. 2009).

<sup>5</sup> IRAF (Image Reduction and Analysis Facility) is distributed by the National Optical Astronomy Observatories, which is operated by the Association of Universities for Research in Astronomy, Inc., under cooperative agreement with National Science Foundation.

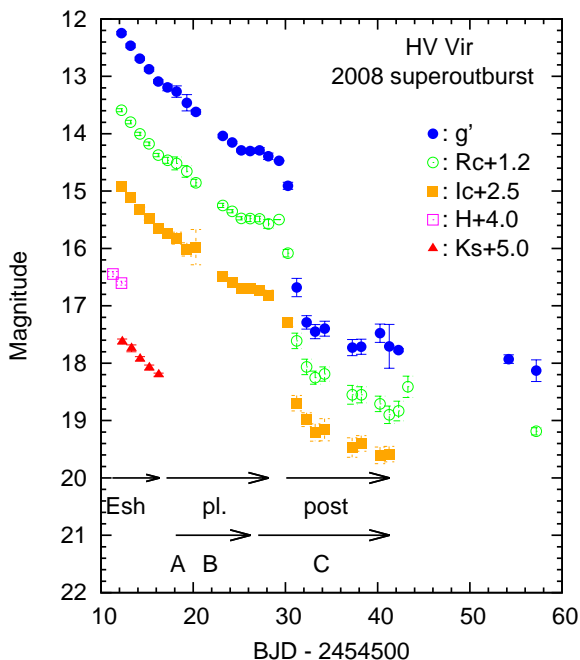


**Fig. 1.** Light curves of HV Vir during the 2008 superoutburst. The obtained data except for  $g'$  band are shifted for display purposes. As noted above, a visual magnitude was fainter than 13.7 on JD 2454510.639, after which the outburst was discovered on JD 2454511.101 with a visual magnitude of 11.5. After the termination of the plateau stage, a long fading tail was observed. No rebrightening was recorded during our run.

### 3.2 period analyses of light curves

We performed period analyses during the plateau stage. After removing the general trend of the light curve, we measured the maximum timings of early and ordinary superhumps. Tables 4 and 5 show the timings of early and ordinary superhump maxima, respectively. A linear regression to the early superhump maxima yields

$$BJD(max) = 2454512.1503(12) + 0.057093(45) \times E1 \quad (4)$$

where  $E1$  is the cycle count since the appearance of early superhumps in our data. As for stage A (JD 2454517.10–18.34), a linear regression to the superhump maxima yields

$$BJD(max) = 2454517.1488(6) + 0.058533(58) \times E2 \quad (5)$$

where  $E2$  is the cycle count since the appearance of ordinary superhumps in our data. Similarly, linear regression to the superhump maxima for stage B (JD 2454519.25–26.21) and C (after JD 2454527.05) yield

$$BJD(max) = 2454517.1188(61) + 0.058500(47) \times E2 \quad (6)$$

for stage B, and

$$BJD(max) = 2454517.2149(50) + 0.057905(20) \times E2 \quad (7)$$

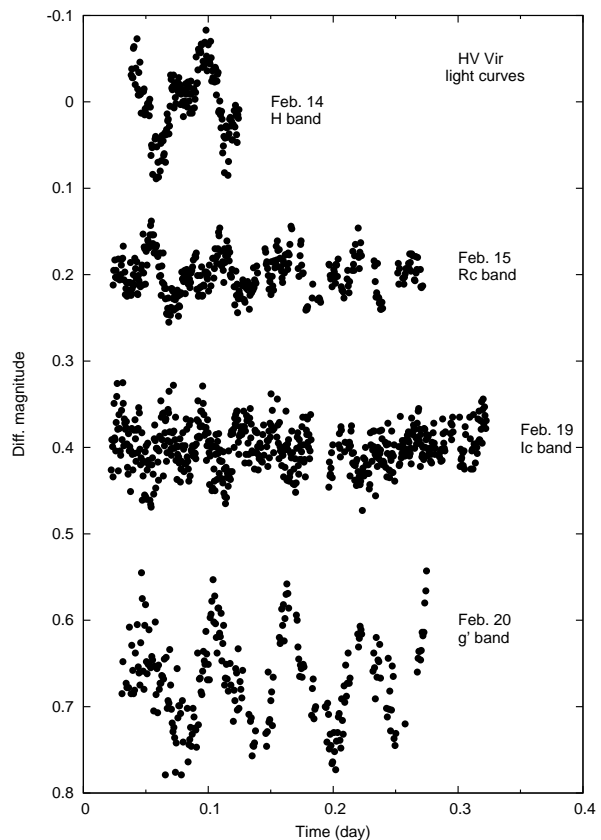


**Fig. 2.** Representative light curves of HV Vir. Early superhumps are visible on February 14, 15, and 19, while ordinary superhumps are seen on February 20. The light curves are arbitrarily shifted for better visualization.

for stage C, respectively. Based on these results, we derived the mean periods of early and ordinary superhumps to be 0.057093(45) d for early superhumps, 0.058533(59) d for stage A superhumps, 0.058500(47) d for stage B superhumps, and 0.057905(20) d for stage C superhumps, respectively. The obtained early superhump period is in agreement with that reported during the 1992 superoutburst ( $P_{\text{Esh}} = 0.057085(23)$  d, Kato et al. (2001)). Also, the mean superhump period during stage A is again in agreement with that during the 2002 superoutburst ( $P_{\text{sh}} = 0.05844(24)$  d, Ishioka et al. (2003)). According to Kato et al. (2009), fractional period excesses during stage A over the mean superhump period during stage B tend to be clustered around 1.0–1.5%. In the present case, however, the mean superhump periods did not differ between stage A and B. This may be due to the fact that our observations of stage B were clustered to the late stage of the superoutburst plateau. As noted in introduction, the stage B superhump period increases as the superoutburst proceeds. Therefore, the mean superhump period during stage B that we obtained in this paper might be overestimated. We summarize the results in table 6.

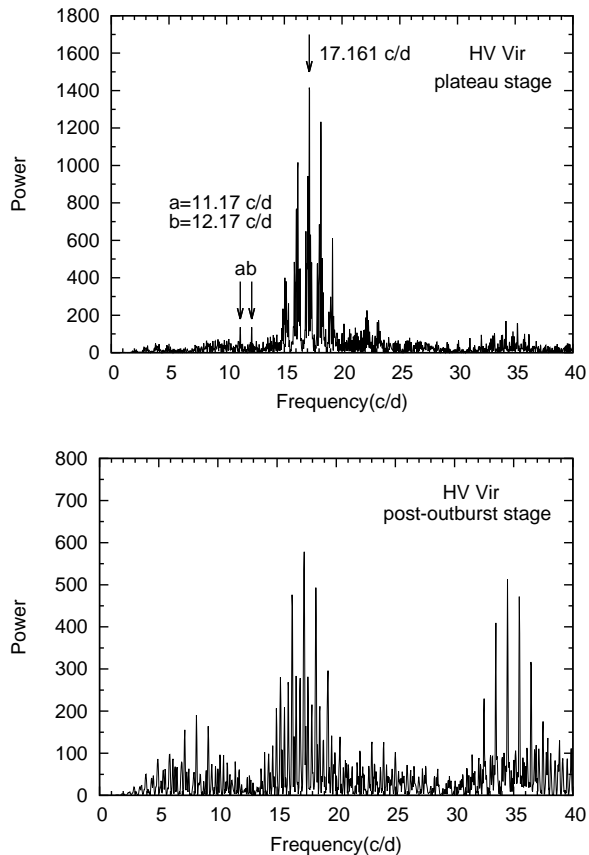


**Fig. 3.** (Left) Discrete Fourier Transform during the main plateau stage after the appearance of superhumps (pl.). The strongest signal corresponds to the mean superhump frequency of 17.16(4) c/d. Weak signals at 11.17(4) and 12.17(4) c/d are detectable. (Right) Discrete Fourier Transform after the end of the main superoutburst. No significant signals around  $\sim 11$  c/d was found.

As noted in introduction, quiescent light curves showed a frequency of 11.20 c/d or 12.21 c/d (Patterson et al. 2003). In order to check whether these signals are present during our observations, we performed Discrete Fourier Transform analyses. Figure 3 shows the results of our analyses. During the plateau stage after the appearance of the superhumps (pl.), we detected weak signals at 11.17(4) and 12.17(5) c/d (0.08953 d and 0.08217 d), which are close to those obtained in Patterson et al. (2003). Similar signals were detected in e.g., FS Aur (Tovmassian et al. 2003), GW Lib (Woudt, Warner 2002), and V455 And (Araujo-Betancor et al. 2005), and SSS J122221.7-311525 (Neustroev et al. 2017). It should be noted that these periods are significantly longer than the orbital ones. On the other hand, we did not detect these signals after the end of the superoutburst, despite the fact that such signals were detected during quiescence in other systems. Because little is known about such a long period of WZ Sge-type dwarf novae, we avoid further discussion on these peri-

**Table 4.** Timings of early superhump maxima of HV Vir.

E1	max	Error
0	4512.1526	0.0009
1	4512.2092	0.0014
2	4512.2602	0.0013
3	4512.3206	0.0025
17	4513.1236	0.0008
18	4513.1776	0.0009
35	4514.1450	0.0008
36	4514.2076	0.0011
37	4514.2630	0.0010
53	4515.1766	0.0012

<sup>†</sup>BJD-2450000.

odicities.<sup>6</sup>

### 3.3 profile of light curves and color variations

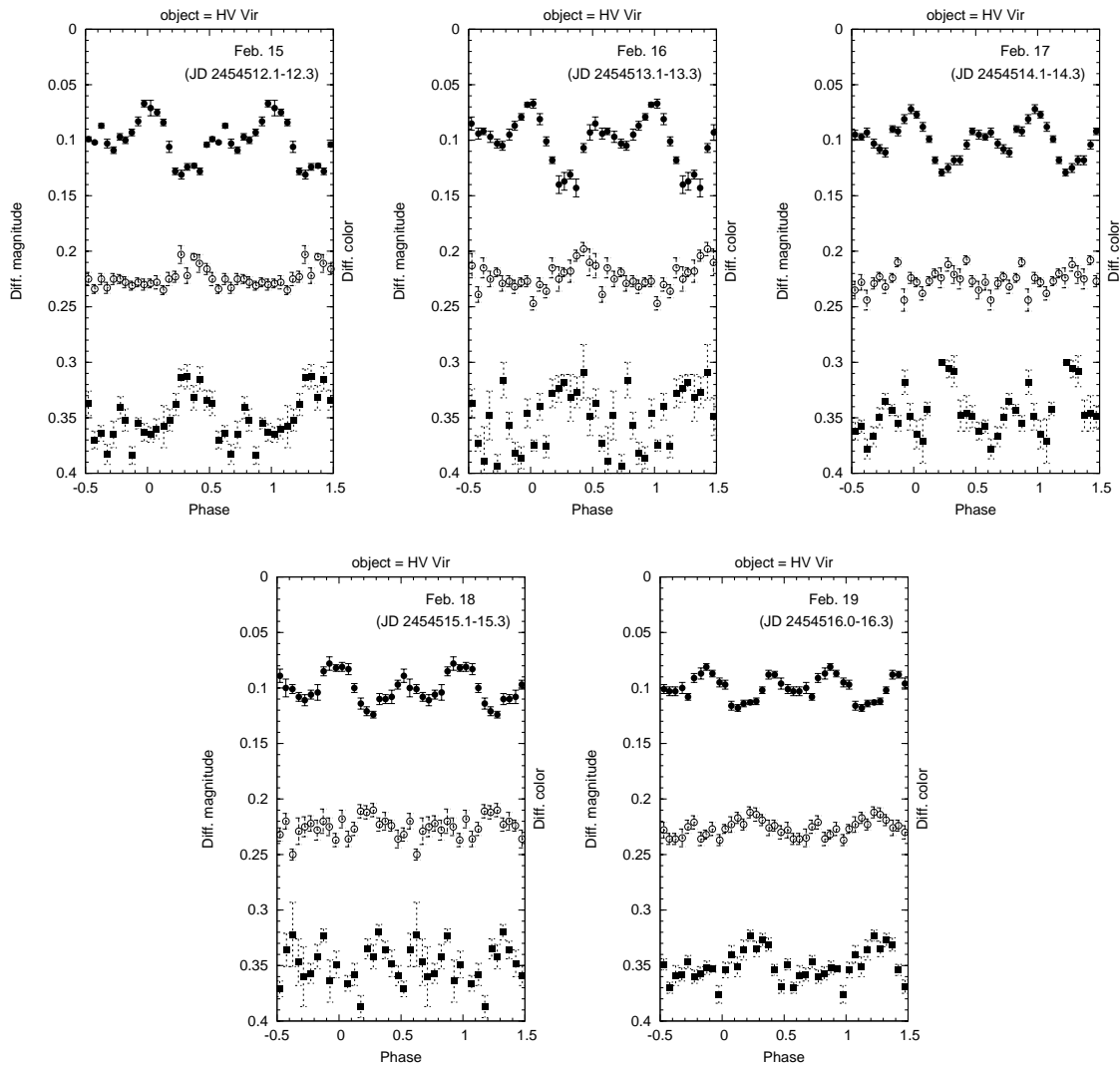
Figure 4 shows  $R_c$  light curves and colors folded with  $P_{\text{Esh}} = 0.057093$  d. Double-peaked modulations characteristic of early superhumps are conspicuous in each panel. In contrast to these light curves, color variations tend to show single-peaked profiles. It should be noted that colors are the bluest at the brightness minima. This property has been reported during the 2007 superoutburst of V455 And (Matsui et al. 2009).

Figure 5 represents  $R_c$  light curves and  $g' - I_c$  color variations folded with  $P_{\text{sh}} = 0.058533$  d for February 20 and 21 (stage A),  $P_{\text{sh}} = 0.058500$  d for February 26–28 (stage B), and  $P_{\text{sh}} = 0.058394$  d for March 1 (stage C). We can see a tendency that  $g' - I_c$  colors are the bluest at the brightness minima on February 21 and 26. As was observed in HV Vir, the difference in phase between magnitudes and colors was also observed in other superhumps, such as e.g., VW Hyi (Schoembs, Vogt 1980), EK TrA (Hassall 1985), and V455 And (Matsui et al. 2009).

### 3.4 amplitudes of early and ordinary superhumps

We studied nightly-averaged amplitudes of each band, which is illustrated in figure 6. It should be noted that the mean amplitudes of early superhumps in near-infrared bands are larger than those in the optical ranges. We can see a tendency that the amplitudes of  $g'$  band show small values over the course of the superoutburst. The amplitudes of early superhumps decreased as the superoutburst proceeded. After the appearance of the superhumps, the maximum of the amplitude occurred on JD 2454518, corresponding to the transition between the

<sup>6</sup> See also Tovmassian et al. (2007) for interpretation of these periodicities.



**Fig. 4.** Light curves and color variations of HV Vir during early superhump stage (Esh). Each panel shows  $R_c$  band (filled circles),  $g' - I_c$  (open circles), and  $g' - K_s$  (filled squares). These data are folded with 0.057093 d and the epoch is set on BJD 2454512.2100. The profiles of the light curves are double-peaked, characteristic of early superhumps. On the other hand, the color variations tend to show single-peaked profiles.

stage A and B. In contrast with the amplitudes of early superhumps, no significant dependency on wavelength was found in ordinary superhumps.

## 4 Results of OT J012059.6+325545

### 4.1 overall light curves

Figure 7 shows  $g'$ ,  $R_c$ , and  $I_c$  band light curves. The light curves closely resemble that observed during the 2001 superoutburst of WZ Sge, in terms of the amplitude of the superoutburst ( $\sim 8$  mag), the duration of the plateau stage ( $\sim 25$  d), and the rebrightenings. The rebrightenings are classified as the type A-B rebrightenings defined by Imada et al. (2006) and Kato (2015). We detected rising stages of the second and third rebrightenings on JD

2455561 and JD 2455563, respectively. The duration of each rebrightening was about 2 d, which is almost the same as that observed during the 2001 superoutburst of WZ Sge itself (Kato et al. 2009). We derived the rising rates of the second and third rebrightenings in  $R_c$  band to be 5.74(11) mag/d and 5.56(14) mag/d, respectively. These values indicate the outside-in type of these rebrightenings (Kato et al. 2004a).

### 4.2 period analyses of light curves

In order to determine the mean periods of early and ordinary superhumps, we calculated maximum timings of humps, which are tabulated in table 7 and 8. A linear regression to the early superhump maxima yields

**Table 5.** Timings of ordinary superhump maxima of HV Vir.

E2	max	Error	Stage
0	4517.1496	0.0007	A
1	4517.2059	0.0005	A
2	4517.2652	0.0005	A
3	4517.3256	0.0006	A
17	4518.1437	0.0008	A-B
18	4518.2024	0.0014	A-B
103	4523.1414	0.0008	B
105	4523.2608	0.0009	B
120	4524.1415	0.0012	B
122	4524.2545	0.0009	B
123	4524.3167	0.0012	B
137	4525.1338	0.0015	B
138	4525.1949	0.0014	B
139	4525.2490	0.0010	B
140	4525.3089	0.0008	B
155	4526.1833	0.0014	B
171	4527.1171	0.0006	C
174	4527.2892	0.0012	C
175	4527.3481	0.0010	C
225	4530.2456	0.0007	C
226	4530.3033	0.0007	C
240	4531.1088	0.0042	C
241	4531.1722	0.0017	C
242	4531.2293	0.0016	C
243	4531.2890	0.0009	C
261	4532.3216	0.0030	C
275	4533.1356	0.0027	C
277	4533.2561	0.0015	C
278	4533.3081	0.0023	C
294	4534.2415	0.0017	C
295	4534.3006	0.0020	C

<sup>†</sup>BJD–2450000.

**Table 6.** Results of period analyses of HV Vir.

Stage*	JD(start-end) <sup>†</sup>	period(day)
Esh	4511.2348–4516.3685	0.057093(45)
A	4517.1018–4518.3470	0.058533(58)
B	4518.1024–4526.2114	0.058500(47)
C	4527.0560–4541.2899	0.057905(20)

\* Esh: Early superhumps.

A: stage A. B: stage B. C: stage C

<sup>†</sup>JD–2450000.

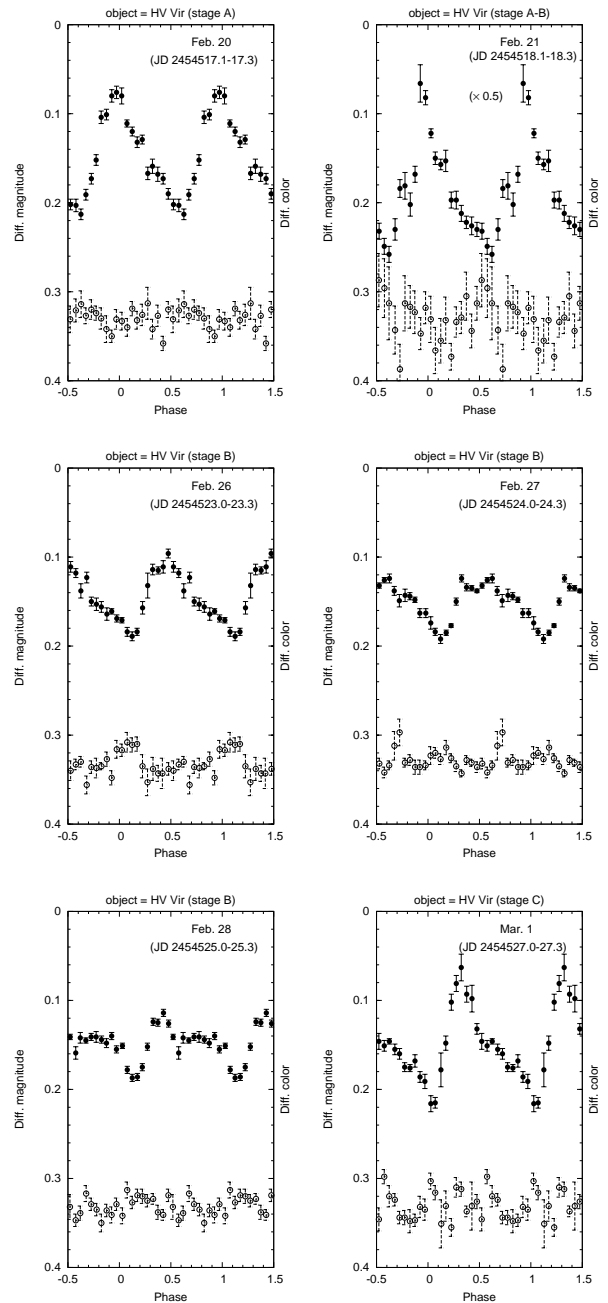


**Fig. 5.**  $R_c$  light curves (filled circles) and  $g' - I_c$  variations (open circles) of HV Vir during the plateau stage. We folded them with 0.058533 d on 2008 February 20 and 21, with 0.058500 d on February 26–28, and 0.057905 d on March 1, respectively. The epoch is set on BJD 2454517.1492. For display purpose, the superhump profile on February 21 is scaled down by 0.5.



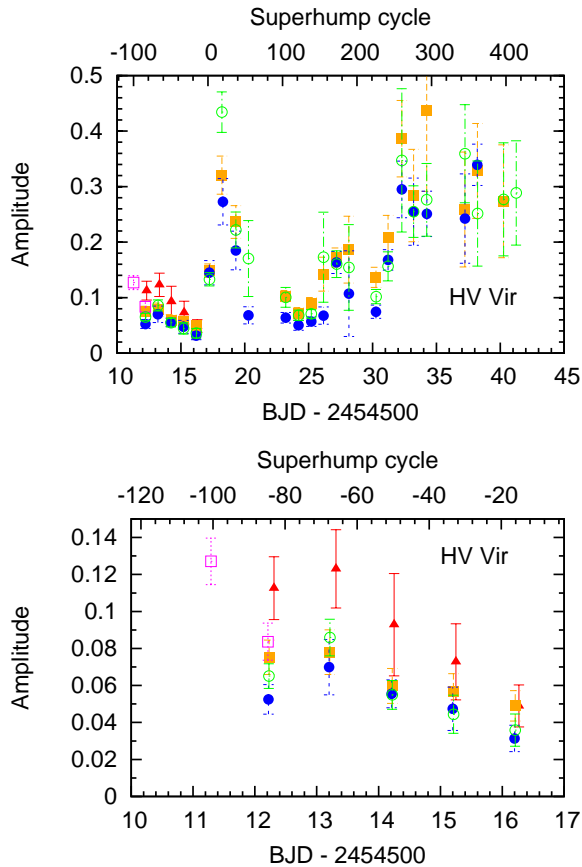


**Fig. 6.** Left: Amplitudes of early and ordinary superhumps of HV Vir. Filled circles (blue), open circles (green), and filled squares (orange) represent data of  $g'$ ,  $R_c$ , and  $I_c$  band, respectively. Near-infrared data are marked with open squares ( $H$  band, magenta) and filled triangles ( $K_s$  band, red), respectively. The amplitudes of superhumps reach a maximum at around the stage A–B transition, after which the amplitudes are decayed until around the stage B–C transition (around JD 2454526). Right: Enlarged figure during the early superhump stage. Note that near-infrared amplitudes are larger than optical amplitudes.

**Table 7.** Timings of early superhump maxima of J0120.

E1	max	Error
0	5533.9262	0.0007
1	5533.9831	0.0006
2	5534.0389	0.0013
18	5534.9529	0.0007
19	5535.0144	0.0014
35	5535.9255	0.0009
36	5535.9803	0.0010
37	5536.0407	0.0009
105	5539.9244	0.0023
106	5539.9852	0.0017

<sup>†</sup>BJD–2450000.

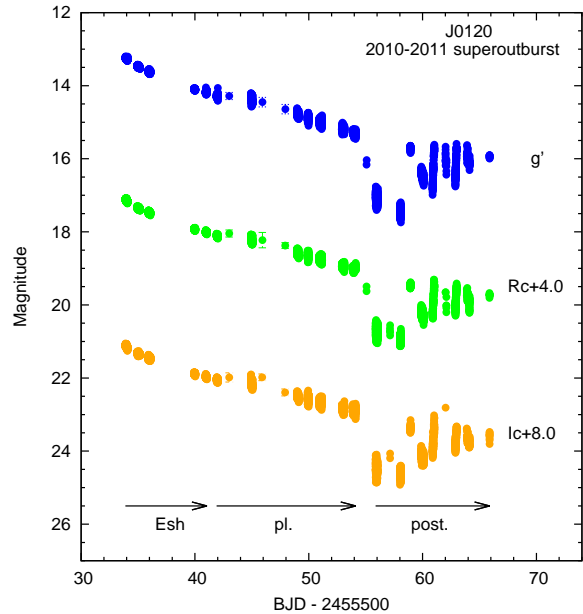


**Fig. 7.**  $g'$  (blue),  $R_c$  (green) and  $I_c$  (orange) light curves of J0120 during the 2010-2011 superoutburst. In combination with the discovery of the superoutburst, the duration of the plateau stage is estimated as long as 25 d. Each light curve clearly shows a "dip" after the end of the plateau stage.

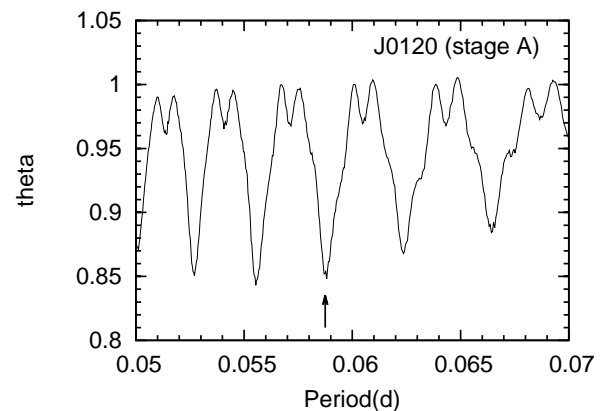


**Fig. 8.** Theta diagram between JD 2455540.9302–43.1383, corresponding to the onset of the growing superhumps. Considering the mean early superhump period of J0120 ( $P_{\text{Esh}} = 0.057147$  d), the best candidate period is 0.05888 d.

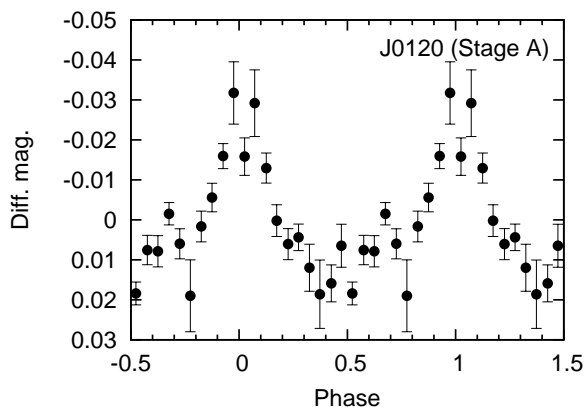


**Fig. 9.** Phase-averaged light curve on 2010 December 10–12 folded with 0.05875 d. The single-peaked light curve is indicative of the growing superhumps.

**Table 8.** Timings of ordinary superhump maxima of J0120.

E2	max	Error	Stage
0	5540.9534	0.0010	A
17	5541.9533	0.0011	A
18	5542.0099	0.0015	A
68	5544.9258	0.0007	B
69	5544.9854	0.0004	B
70	5545.0418	0.0004	B
139	5549.0247	0.0007	B
155	5549.9509	0.0009	B
172	5550.9305	0.0006	B
173	5550.9888	0.0011	B
174	5551.0452	0.0008	B
175	5551.1026	0.0019	B

<sup>†</sup>BJD–2450000.

**Table 9.** Results of period analyses of J0120.

Stage*	JD(start-end) <sup>†</sup>	period(day)
Esh	5533.8857–5541.0535	0.057147(15)
A	5540.9302–5543.1383	0.05875(11)
B	5544.9190–5554.1251	0.057729(8)

\* Esh: Early superhumps.

A: stage A. B: stage B.

<sup>†</sup>JD–2450000.

$$BJD(max) = 2455533.9256(8) + 0.057147(15) \times E1, \quad (8)$$

where  $E1$  is the cycle count since the appearance of early superhumps in our data. Based on the regression analysis, we derived the mean early superhump period to be  $P_{Esh} = 0.057147(15)$  d.

Nakagawa et al. (2013) reported that a hint of growing superhumps (stage A superhumps) was observed around JD 2454442.0. In order to confirm this, we performed the phase dispersion minimization method (PDM, Stellingwerf (1978)) on JD 2455540.93–43.13. The resulting theta diagram is shown in figure 8. In this diagram, we can detect several peaks, of which  $P = 0.05888(11)$  d is the best candidate period, based on the fact that the mean superhump period is slightly longer than the orbital period (or  $P_{Esh}$ ) of the system (Kato 2015). Our regression analyses yield

$$BJD(max) = 2455540.9535(15) + 0.05875(11) \times E2 \quad (9)$$

for JD 2455540.93–43.13, and

$$BJD(max) = 2455540.9434(11) + 0.057729(8) \times E2 \quad (10)$$

for JD 2455544.91–54.12, respectively. The estimated period between JD 2455540.93–43.13 ( $P_{sh} = 0.05875(11)$  d) is in agreement with that derived by the PDM ( $P_{sh} = 0.05888(11)$  d). On the other hand, the mean superhump period for JD 2455544.91–54.12 was shorter than that obtained by Nakagawa et al. (2013) ( $P_{sh} = 0.057814(12)$  d) by 0.15 %. This difference may be caused by the fact that the different baselines were used for determining the mean superhump period, and the fact that  $P_{sh}$  varies as the superoutburst proceeds (Kato et al. 2009). It should be noted that the mean superhump period between JD 2455540.93–43.13 is about 1.8% longer than that between JD 2455544.91–54.12. Such a long periodicity after the end of early superhumps is characteristic of stage A superhumps (Kato et al. 2009). Figure 9 shows  $R_c$  light curve folded with  $P_{sh} = 0.05875$  d, in which a single-peaked modulation, characteristic of superhumps, is visible. Therefore, it is likely that the observed modulations between JD 2455540.93–43.13 are indeed stage A superhumps. We summarize our period analyses of J0120 in table 9.

Kato, Osaki (2013) developed a new method for estimating the mass ratio of the system using the orbital and stage A superhump periods. Empirically,  $P_{Esh}$  is identical with the orbital period of the system (Kato 2015). Here we regard  $P_{Esh}$  as  $P_{orb}$  and estimated the mass ratio to be  $q = 0.073(7)$ . The error of the mass ratio is estimated based on the analytic formulae of Kato, Osaki (2013), the error of the stage A superhump period, and that of the early superhump period. The estimated mass ratio is common

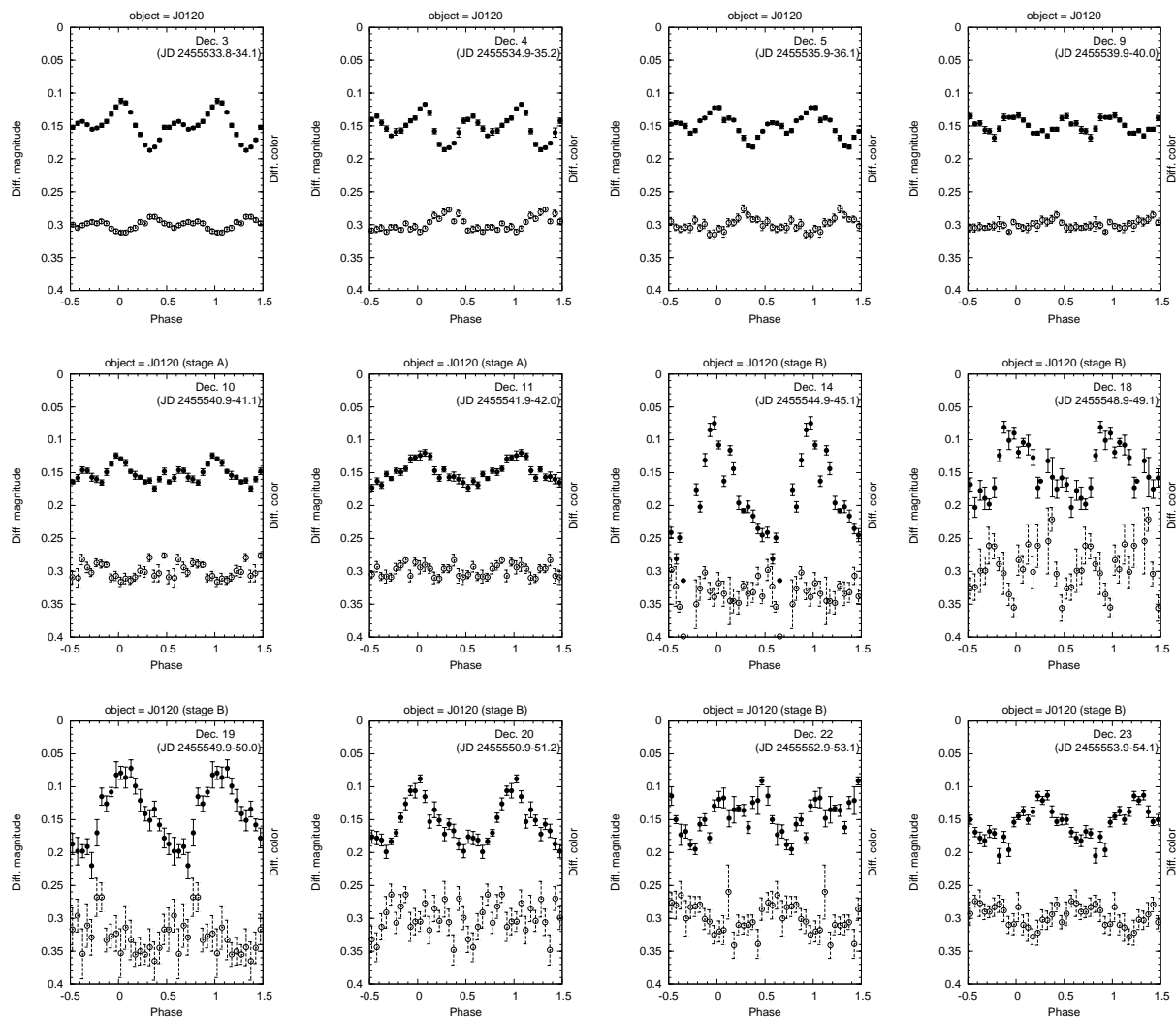


**Fig. 10.**  $R_c$  light curves (filled circles) and  $g' - I_c$  variations (open circles). These data are folded with 0.057147 d (December 3–9), 0.05875 d (December 10–11) and 0.057834 d (after December 14), respectively. The epoch is set on BJD 2455544.4060.

among WZ Sge-type dwarf novae (Kato 2015). The validity of the obtained mass ratio should be tested by future spectroscopic observations.

### 4.3 profiles of humps and color variations

Figure 10 shows  $R_c$  nightly-averaged light curves and  $g' - I_c$  variations folded with the above obtained periods. Here we precluded several nights data with low quality and short observations. Although the profiles of early superhumps vary from night to night, double-peaked light curves are visible until 2010 December 9 (JD 2455540.02). In the most of the panels during the early superhump stage, the bluest peak in  $g' - I_c$  occurs when  $R_c$  is the faintest, similar to that observed in HV Vir and other WZ Sge-type dwarf novae (Matsui et al. 2009; Neustroev et al. 2017). The  $g' - I_c$  color variations of

ordinary superhumps are not noticeable compared with those of early superhumps, but the bluest peaks correspond to the superhump minima in 2010 December 19 (JD 2455549.89–49.99) 22 (JD 2455552.89–53.12), and 23 (JD 2455553.87–54.12).

Figure 11 shows the evolution of amplitudes of variability in each band. It should be noted that, on the first three nights of our observations, the amplitudes of early superhumps are the largest in  $I_c$  band and the smallest in  $g'$  band. The amplitudes of early superhumps decreased as the outburst proceeded. On the other hand, the amplitudes of ordinary superhumps seems to be independent of wavelength.

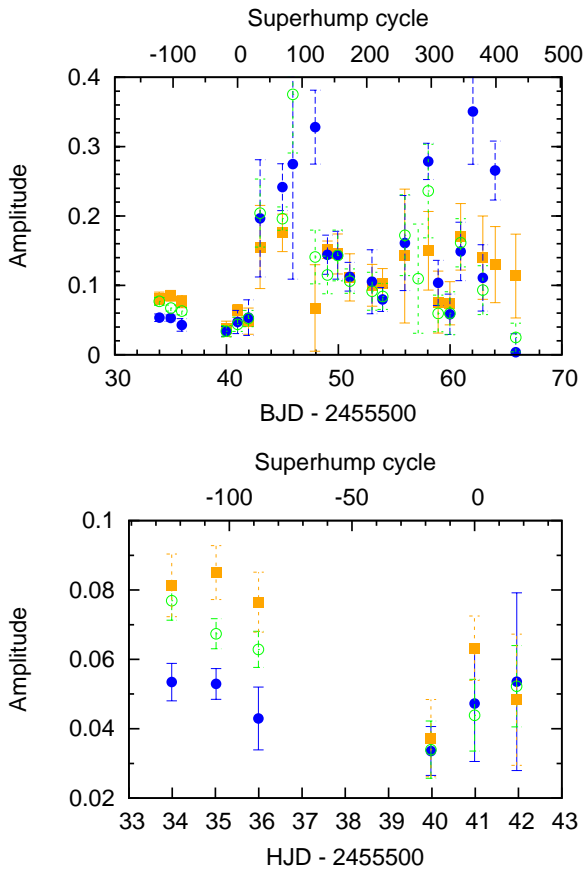


**Fig. 11.** Left: Amplitudes of early and ordinary superhumps of J0120. Filled circles (blue), open circles (green), and filled squares (orange) represent data of  $g'$ ,  $R_c$ , and  $I_c$  band, respectively. The maximum amplitude occurred around the stage A–B transition (around BJD 2455543), after which the amplitudes gradually decreased until the end of the plateau stage. Right: enlarged figure during the early superhump phase. The amplitudes of early superhumps decrease as the superoutburst proceeds. The amplitudes of early superhumps depend on wavelength, particularly on the first three nights of our observations.

## 5 Discussion

As described in the previous section, the amplitudes of early superhumps are different in different bands. For example,  $H$  and  $K_s$  amplitudes in HV Vir showed larger values compared with optical amplitudes, particularly in the first half of the early superhump stage. As for J0120, we can see a tendency that the amplitudes of early superhumps are the largest in  $I_c$  band and the smallest in  $g'$  band for the first three nights of our observations. In general,  $g'$  band amplitudes tend to show small values.

Although the working mechanism on early superhumps is still in debate, theoretical works suggest that the outer region of the accretion disk plays a significant role in producing early superhumps (Nogami et al. 1997; Kato 2002; Uemura et al. 2012). From the observational point of view, the light sources of early super-

**Table 10.**  $\Delta$  of each object at different stages.

Object	stage A	stage B	stage C
HV Vir	0.2	0.4	1
J0120	0.6	0.4	-
J1222	0.3	0.6~1	1

J1222 = SSS J122221.7–311525

humps are likely to have dependence on the system inclination. For example, only very low-amplitude modulations were seen at the early phase of the 2007 superoutburst of GW Lib (Kato et al. 2009), whose inclination is estimated as  $11^\circ$  (Thorstensen et al. 2002). In combination with the previous works, our findings suggest the presence of vertically-expanded cool components at the outer region of the accretion disk during the appearance of the early superhumps, as suggested by Matsui et al. (2009) and Nakagawa et al. (2013).

We find that the amplitudes of ordinary superhumps have no dependence on wavelength. Kato et al. (2012a) showed that amplitudes of superhumps are independent of inclination for not more than  $80^\circ$ . On the other hand, systems with inclination higher than  $80^\circ$  show strong dependence on  $i$  (see figure 90 of Kato et al. 2012a). Based on these results, Kato et al. (2012a) suggest that the vertical structure in the superhump-light source is smaller than  $10^\circ$  in slope against the remaining disk. Taking Kato et al. (2012a) into consideration, our findings imply that the superhump light sources of HV Vir and J0120 are free of self-obscuration of the accretion disk. Because multicolor photometry of superhumps have been performed for only a few systems, we should collect further samples in order to better understand the light source of superhumps.

As illustrated in figure 4, 5, and 10, we can notice the differences between the peaks of the light curves and colors in many panels. In early superhumps, the colors are at the bluest when the magnitudes are at the faintest. This trend is remarkably similar to that reported by Matsui et al. (2009) during the 2007 superoutburst of V455 And. Matsui et al. (2009) suggest that the temperature of the early superhump light source is lower than that of an underlying component. The present studies may further support the idea that the early superhump light source is a low-temperature, vertically expanded region at the outermost part of the accretion disk.

Regarding the ordinary superhumps, Matsui et al. (2009) reported that the bluest peak of the superhumps is prior to the maximum magnitude by phase of 0.15, and the reddest color corresponds to the bright minimum of the superhumps in phase. In contrast with Matsui et al. (2009), such color variations were not found in our

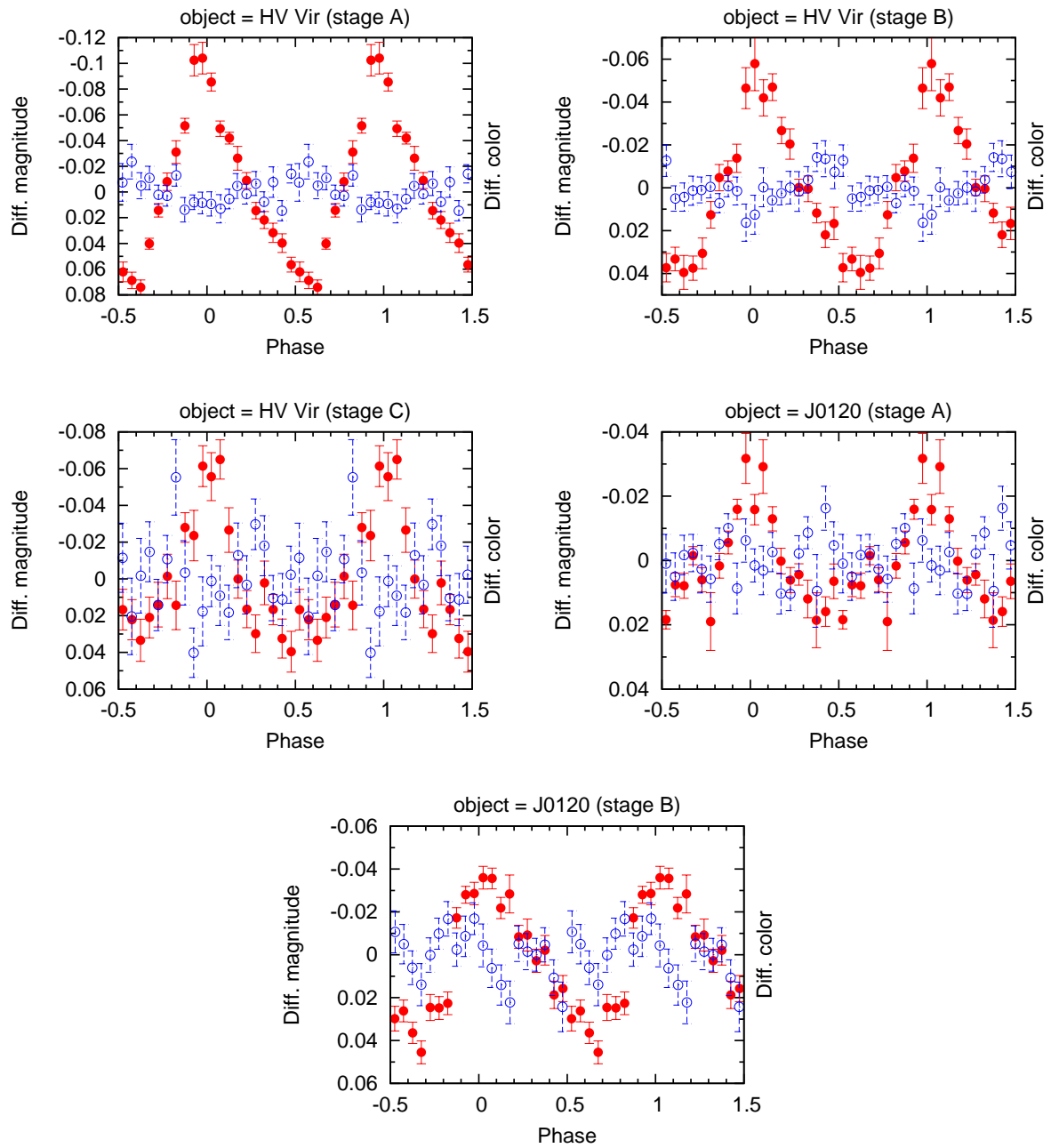
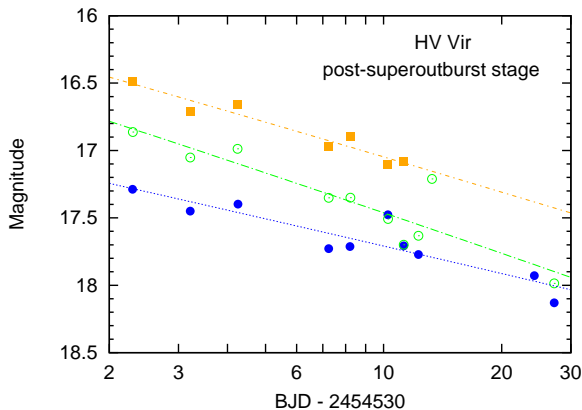


Fig. 12. Averaged profiles of superhumps and colors at different stages. Filled red circles represent superhumps in  $R_c$  band, while opened blue circles represent  $g' - I_c$  color variations.



**Fig. 13.**  $g'$  (blue),  $R_c$  (green), and  $I_c$  (orange) light curves of the post-superoutburst stage of HV Vir. The abscissa denote the date in logarithmic scale since BJD 2454530, corresponding to the beginning of the rapid declining stage, and the ordinate denotes the magnitude of each band. The linear lines in the figure mean the best-fitting power-law functions. Note that the  $g'$  and  $R_c$  band light curves show moderate declines.

study. Neustroev et al. (2017) recently published  $B$ ,  $V$ ,  $R$ , and  $I$  photometry of the WZ Sge-type dwarf nova SSS J122221.7–311525 during the superoutburst, in which they studied color variations of the superhumps according to the stages. Neustroev et al. (2017) point out that color variations are weak in stage A, whereas the bluest peaks correspond to the minimum magnitudes in stage B. As can be seen in figure 5 and 10, some of our panels have a tendency that Neustroev et al. (2017) noted on. In figure 5 and 10, color variations are weak during stage A on February 20, December 10, and 11, despite the fact that the brightness amplitudes of stage A superhumps are the largest among the three stages (Kato et al. 2009). Also, the bluest peaks tend to coincide with the minimum magnitudes during stage B on February 26, 28, December 19, 22 and 23, and during stage A-B transition on February 21. In this respect, the color variations during the superhumps are in accordance with those reported by Neustroev et al. (2017).

In order to further examine the relation between superhump light curves and color variations, and compare our results with figure 9 of Neustroev et al. (2017), we made phase-averaged profiles of them in each stage, which are shown in figure 12. Here we define the amplitude ratio of color variations against superhump variations as  $\Delta$ .<sup>7</sup> We can roughly estimate  $\Delta$  of HV Vir to be 0.2 for stage A, 0.4 for stage B, and 1 for stage C, respectively. As for J0120, we obtained 0.6 for stage A and 0.4 for stage B, respectively. Using figure 9 of Neustroev et al. (2017), we roughly estimated  $\Delta$  of J122221.7–311525 to be 0.3 for

stage A, 0.6 for the first half of stage B, 1 for the second half of stage B, and 1 for stage C, respectively. We summarize  $\Delta$  of each object at different stages in table 10. Although  $\Delta$  for stage A of J0120 deviates from the other values, generally,  $\Delta$  might be around 0.3 for stage A and larger than 0.4 for stage B. Our obtained values imply that stage B and C superhumps tend to show drastic color variations compared with stage A ones.

From the theoretical point, Osaki, Kato (2013b) proposed that the observed superhump period is determined mainly by three factors: dynamical precession, pressure effect, and wave-wave interaction. The wave-wave interaction is negligible compared with the other two factors. At the beginning of the appearance of ordinary superhumps, the pressure effect is immature so that this is negligible as well. As a result, the growing superhumps (stage A) can be regarded as the dynamical precession rate at the 3:1 resonance radius (Osaki, Kato 2013b). As the superoutburst proceeds, the pressure effect becomes dominant, which may be observed as stage B superhumps. Because the pressure effect leads to complicated physical processes in the accretion disk, we can expect that the color variations in stage B show diversity. On the other hand, a weak pressure effect causes the disk to show weak color variations, which may be observed as weak color variations in stage A superhumps. The observed color variations in WZ Sge-type dwarf novae to date seem to be consistent with our interpretation.

Neustroev et al. (2017) investigated the post-superoutburst stage of J1222 and found that all the light curves are described by a broken power law. For example,  $V$  band light curve in J1222 showed a break around  $T \sim 18$ , where  $T$  is the day after the beginning of the rapid fading stage. Neustroev et al. (2017) noted that the origin of a broken power-law decline is unclear, because of the lacking of papers both from the observational and theoretical points of view. In order to compare our results with those reported by Neustroev et al. (2017) in J1222, we examined the post-superoutburst stage of HV Vir.<sup>8</sup> Figure 13 represents  $g'$ ,  $R_c$ , and  $I_c$  light curves during the post-superoutburst stage of HV Vir. Because of the apparent lack of the observations, we were unable to find a break in the light curves. Nevertheless, we calculated power-law indices of each band by fitting the light curves in units of flux. The obtained power-law indices were  $-0.25(4)$  in  $g'$  band,  $-0.37(6)$  in  $R_c$  band, and  $-0.33(4)$  in  $I_c$  band, respectively. The obtained power-law index in  $I_c$  band of HV Vir is close to that of J1222 ( $-0.38(3)$ , Neustroev et al. (2017)). On the other hand, the

<sup>7</sup> For example, if the amplitude of color variation is 0.03 mag and the amplitude of superhumps is 0.2 mag, then  $\Delta$  is  $0.03/0.2 = 0.15$ .

<sup>8</sup> Due to the lack of the data of J0120 during the post-superoutburst stage, we only focused on HV Vir.

power-law indices in  $g'$  and  $R_c$  bands of HV Vir differ from those derived by Neustroev et al. (2017) in J1222, who obtained  $-0.58(3)$  in  $B$  band,  $-0.64(1)$  in  $V$  band, and  $-0.54(2)$  in  $R$  band, respectively. Overall, it should be noted that J1222 showed steep declines in  $B$ ,  $V$ , and  $R$  bands whereas HV Vir showed moderate declines in  $g'$  and  $R_c$  bands. At present, it is unclear what causes such a difference between J1222 and HV Vir, although an apparent difference between them is that J1222 shows the type-E light curve and HV Vir shows the type-D one (Kato et al. 2013b; Kato 2015). Further multicolor photometric studies are desirable in order to understand behavior of the post-superoutburst stage of WZ Sge-type dwarf novae.

## 6 Summary

We summarize our results as follows:

- We detected early superhump periods of  $P_{\text{Esh}} = 0.057093(45)$  d for HV Vir and  $P_{\text{Esh}} = 0.057147(15)$  d for J0120, respectively. The brightness minima of early superhumps correspond to the bluest peaks of color variations.
- The amplitudes of early superhumps have dependence on wavelength. The amplitudes in the near-infrared range are larger than those in the optical range.  $K_s$  band shows the largest amplitudes while  $g'$  band tends to show smaller amplitudes. This indicates that the early superhump light source is low-temperature and generated at the outer region of a vertically-extended accretion disk.
- The amplitudes of ordinary superhumps seem to be independent of wavelength. This implies that the light source of ordinary superhumps are free of self-obscuration of the accretion disk. The superhump light source may be geometrically thin.
- The bluest peaks of ordinary superhumps tend to coincide with the brightness minima. This tendency seems to be evident in stage B superhumps. On the other hand, color variations during stage A are weak. This may reflect significant pressure effects in stage B superhumps.
- We obtained the power-law indices of HV Vir during the post-superoutburst stage and found that  $g'$  and  $R_c$  bands showed moderate declining rates compared with  $I_c$  band. This behavior is in contrast with that observed in a candidate period bouncer SSS J122221.7–311525. The cause of the difference should be clarified by further multicolor photometry of WZ Sge-type dwarf novae during the post-superoutburst stage.

## Acknowledgments

We thank the anonymous referee for valuable comments on the manuscript of the paper. We acknowledge with thanks the variable star observations from the AAVSO and VSNET International Database contributed by observers worldwide and used in this research.

## References

- Ahn, C. P., et al. 2012, *ApJS*, 203, 21  
 Araujo-Betancor, S., et al. 2005, *A&A*, 430, 629  
 Barwig, H., Mantel, K. H., & Ritter, H. 1992, *A&A*, 266, L5  
 Drake, A. J., et al. 2009, *ApJ*, 696, 870  
 Hassall, B. J. M. 1985, *MNRAS*, 216, 335  
 Hellier, C. 2001, *Cataclysmic Variable Stars: How and why they vary* (Berlin: Springer-Verlag)  
 Hirose, M., & Osaki, Y. 1990, *PASJ*, 42, 135  
 Howell, S. B., Szkody, P., & Cannizzo, J. K. 1995, *ApJ*, 439, 337  
 Imada, A., Kubota, K., Kato, T., Nogami, D., Maehara, H., Nakajima, K., Uemura, M., & Ishioka, R. 2006, *PASJ*, 58, L23  
 Ishioka, R., et al. 2001, *PASJ*, 53, 905  
 Ishioka, R., et al. 2003, *PASJ*, 55, 683  
 Isogai, M., Arai, A., Yonehara, A., Kawakita, H., Uemura, M., & Nogami, D. 2015, *PASJ*, 67, 7  
 Kato, T. 2002, *PASJ*, 54, L11  
 Kato, T. 2015, *PASJ*, 67, 108  
 Kato, T., et al. 2013a, *PASJ*, 65, 23  
 Kato, T., et al. 2009, *PASJ*, 61, S395  
 Kato, T., et al. 2012a, *PASJ*, 64, 21  
 Kato, T., Maehara, H., & Uemura, M. 2012b, *PASJ*, 64, 62  
 Kato, T., Monard, B., Hamsch, F.-J., Kiyota, S., & Maehara, H. 2013b, *PASJ*, 65, L11  
 Kato, T., Nogami, D., Matsumoto, K., & Baba, H. 2004a, *PASJ*, 56, S109  
 Kato, T., & Osaki, Y. 2013, *PASJ*, 65, 115  
 Kato, T., Sekine, Y., & Hirata, R. 2001, *PASJ*, 53, 1191  
 Kato, T., Uemura, M., Ishioka, R., Nogami, D., Kunjaya, C., Baba, H., & Yamaoka, H. 2004b, *PASJ*, 56, S1  
 Kato, T. et al. 2017, *PASJ*, 69, 75  
 Kotani, T., et al. 2005, *Nuovo Cimento C Geophysics Space Physics C*, 28, 755  
 Lasota, J.-P. 2001, 45, 449  
 Leibowitz, E. M., Mendelson, H., Bruch, A., Duerbeck, H. W., Seitter, W. C., & Richter, G. A. 1994, *ApJ*, 421, 771  
 Lipunov, V., et al. 2010, *Advances in Astronomy*, 2010, 349171  
 Matsui, R., et al. 2009, *PASJ*, 61, 1081  
 Meyer, F., & Meyer-Hofmeister, E. 1981, *A&A*, 104, L10  
 Nakagawa, S., Noguchi, R., Iino, E., Ogura, K., Matsumoto, K., Arai, A., Isogai, M., & Uemura, M. 2013, *PASJ*, 65, 70  
 Neustroev, V. V., et al. 2017, *MNRAS*, 467, 597  
 Nogami, D., Kato, T., Baba, H., Matsumoto, K., Arimoto, J., Tanabe, K., & Ishikawa, K. 1997, *ApJ*, 490, 840  
 Osaki, Y. 1989, *PASJ*, 41, 1005  
 Osaki, Y. 1996, *PASP*, 108, 39  
 Osaki, Y., & Kato, T. 2013a, *PASJ*, 65, 50  
 Osaki, Y., & Kato, T. 2013b, *PASJ*, 65, 95  
 Osaki, Y., & Meyer, F. 2002, *A&A*, 383, 574

- Patterson, J. 2011, MNRAS, 411, 2695
- Patterson, J., et al. 1998, PASP, 110, 1290
- Patterson, J., et al. 2002, PASP, 114, 721
- Patterson, J., et al. 2003, PASP, 115, 1308
- Ritter, H., & Kolb, U. 2003, A&A, 404, 301
- Schoembs, R., & Vogt, N. 1980, A&A, 91, 25
- Shappee, B. J., et al. 2014, ApJ, 788, 48
- Smak, J. 1984, Acta, Astron, 34, 161
- Smith, J. A., et al. 2002, AJ, 123, 2121
- Stellingwerf, R. F. 1978, ApJ, 224, 953
- Szkody, P., Gänsicke, B. T., Sion, E. M., & Howell, S. B. 2002, ApJ, 574, 950
- Thorstensen, J. R. 2003, 126, 3017
- Thorstensen, J. R., Patterson, J. O., Kemp, J., & Vennes, S. 2002, PASP, 114, 1108
- Tovmassian, G., et al. 2003, PASP, 115, 725
- Tovmassian, G. H., Zharikov, S. V., & Neustroev, V. V. 2007, ApJ, 655, 466
- Uemura, M., et al. 2008, PASJ, 60, 227
- Uemura, M., Kato, T., Ohshima, T., & Maehara, H. 2012, PASJ, 64, 92
- Warner, B. 1995, Cataclysmic Variable Stars (Cambridge: Cambridge University Press)
- Whitehurst, R. 1988, MNRAS, 232, 35
- Woudt, P. A., & Warner, B. 2002, 282, 433
- Woudt, P. A., Warner, B., de Budé, D., Macfarlane, S., Schurch, M. P. E., & Zietsman, E. 2012, MNRAS, 421, 2414
- Yanagisawa, K., et al. 2006, SPIE, 6269, 62693Q